On the Geometric Foundations of Complex Dynamics

Ervin Goldfain

Global Institute for Research, Education and Scholarship (GIRES), USA

ervingoldfain@gmail.com

July 1, 2026

Abstract

Physical systems driven far from thermodynamic equilibrium generically develop self-similar, fractal structures that cannot be described by conventional Riemannian geometry. We present a guide to the geometric and statistical tools needed to characterize such structures, progressing from Hölder exponents and invariant (SRB) measures through Hausdorff dimension, the multifractal formalism, and the singularity spectrum $f(\alpha)$. Universal routes to chaos — period-doubling (Feigenbaum), quasiperiodicity, and intermittency (Pomeau–Manneville) — are analyzed through the renormalization group (RG) techniques, each producing a distinct multifractal attractor. Generalized Rényi and Tsallis entropies capture the non-extensive statistics at the edge of chaos, while dimensional flow describes how the effective spacetime dimension runs with the observation scale. Large Deviation Theory is shown to unify these concepts, providing the exponential statistics of rare fluctuations and a microscopic derivation of the Second Law. Throughout, we emphasize the deep connections of these ideas to foundational physics: the generation structure of the Standard Model (SM) emerges from the Feigenbaum cascade in the chaotic limit of the RG flow; the Minimal Fractal Manifold (MFM) provides a ultraviolet (UV) completion of quantum field theory without new symmetries; the Complex Ginzburg–Landau equation (CGLE) bridges complex dynamics to classical field theory and General Relativity (GR); while topological condensation of continuous dimensions offers a geometric model of dark matter. Seven original figures — bifurcation diagrams, the singularity spectrum, SRB measure plots, route-to-chaos time series, rate functions, dimensional flow, and RG phase portraits — are included to make the presentation self-contained.

Keywords: multifractals; Hölder exponents; Hausdorff dimension; singularity spectrum; Feigenbaum universality; generalized entropies; dimensional flow; large deviation theory; renormalization group; Standard Model; fractal spacetime; complex Ginzburg–Landau equation; dark matter.

Contents

1. Introduction

Classical and quantum field theories are built on the premise that the vacuum is a uniform and continuous Minkowski or de Sitter background. Yet every quantum field theory (QFT) in four dimensions requires ultraviolet (UV) regularization, signaling that this uniform continuity breaks down at short distances. The renormalization group (RG) equations of QFT describe a *flow* of coupling constants with the energy scale μ — which behave as nonlinear dynamical systems. From this standpoint, the RG flow can become chaotic in the near or far ultraviolet (UV), and the resulting *multifractal* structure of coupling space and spacetime encodes the observed spectrum of SM parameters [1–11].

This paper provides a guide to the mathematical toolkit underlying this perspective. The presentation is structured to be self-contained and to emphasize physical intuition at every step, with mathematical definitions accompanied by their dynamical meaning. Figure 1 below provides a road map of the main concepts and their interconnections. The paper proceeds from local orbit statistics (Sections 2–3), through global geometric structure (Sections 4–5), to universal dynamics (Section 6), statistical tools (Sections 7–8), and the connections to foundational physics (Section 9).

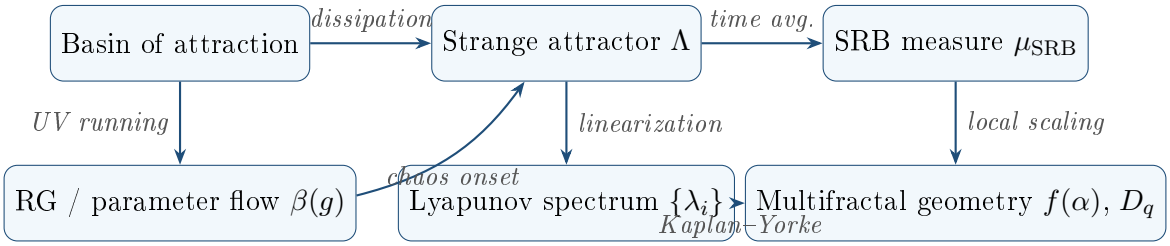

Figure 1: Conceptual map of the key objects and relationships developed in this paper. A dissipative nonlinear flow contracts phase-space volume onto a strange attractor Λ. Orbit time-averages define the SRB measure μ_{SRB}, whose local scaling properties encode the multifractal geometry $f(\alpha)$. The Kaplan–Yorke formula connects the Lyapunov spectrum $\{\lambda_i\}$ to the Hausdorff dimension of μ_{SRB}. In the field-theory context (right column), the renormalization-group (RG) flow plays the role of the dynamical system, and its UV chaotic attractor generates the multifractal structure of coupling space and spacetime.

2. Invariant Measures and Hölder Exponents

2.1 What the orbit actually measures: the SRB distribution

Consider a dissipative nonlinear system — a laser, a driven pendulum, or a coupled set of RG equations. After transients die out, almost every trajectory settles onto an attractor Λ. The orbit wanders over Λ forever, but not uniformly: some regions are visited far more frequently than others. This non-uniform visitation pattern defines the *Sinai–Ruelle–Bowen (SRB) measure* [13–16]:

$$\lim_{T\to\infty} \frac{1}{T} \int_0^T \delta_{\varphi_t(x)}\, dt \;=\; \mu_{\mathrm{SRB}} \qquad \text{for Lebesgue-a.e. initial condition } x. \tag{1}$$

Two terms in eq. (1) deserve a brief explanation. $\delta_{\varphi_t(x)}$ is the Dirac delta mass concentrated at the moving orbit point $\varphi_t(x)$; the time integral accumulates these point masses into a probability measure whose weight on any region A equals the fraction of time the orbit spends in A. *Lebesgue-almost-everywhere* (Lebesgue-a.e.) means: for every initial condition x except possibly a set of zero phase-space volume — in practice, for virtually any starting point one could choose.

Equation (1) says that time averages of any observable g converge to $\int g\, d\mu_{\mathrm{SRB}}$, regardless of which initial condition you start from (as long as it is in the basin). The SRB measure is the natural *nonequilibrium* analog for the Gibbs measure: it describes the statistical state of a deterministic system in its long-time asymptotics.

> **Physical meaning.** $\mu_{\mathrm{SRB}}(A)$ = fraction of time a typical orbit spends in region A. It is the "natural" probability distribution induced by the dynamics, and is the correct measure to use when computing expectation values, entropies, and correlation functions on a chaotic attractor.

2.2 Hölder exponents: local clustering of orbits

Zoom into a small ball $B(x,\varepsilon)$ of radius ε around a point x on the attractor. The SRB measure of that ball, $\mu_{\mathrm{SRB}}(B(x,\varepsilon))$, tells you how densely the orbit clusters near x. The *local Hölder (scaling) exponent* captures how this density scales with the resolution:

$$\boxed{\alpha(x) \;=\; \lim_{\varepsilon\to 0} \frac{\log \mu(B(x,\varepsilon))}{\log \varepsilon},} \tag{2}$$

so that $\mu(B(x,\varepsilon)) \sim \varepsilon^{\alpha(x)}$ as $\varepsilon \to 0$. Large α means dilute (rarely visited); small α means concentrated (frequently visited). The connection to physics is direct:

$$\alpha(x) \;\simeq\; \frac{1}{\lambda_{\mathrm{loc}}(x)}, \tag{3}$$

where $\lambda_{\mathrm{loc}}(x)$ is the local (finite-time) Lyapunov exponent at x. Points with rapid local expansion (λ_{loc} large) have *small* α (high density, frequently visited) according to eq. (3); conversely, intermittent "sticky" regions (λ_{loc} small) correspond to *large* α (low density, rarely visited).

Figure 2 illustrates these ideas for the logistic map when the control parameter is $r = r_\infty$: the SRB measure is highly non-uniform (panel a), and the corresponding distribution of local Hölder exponents spans a finite range (panel b) — the hallmark of multifractality.

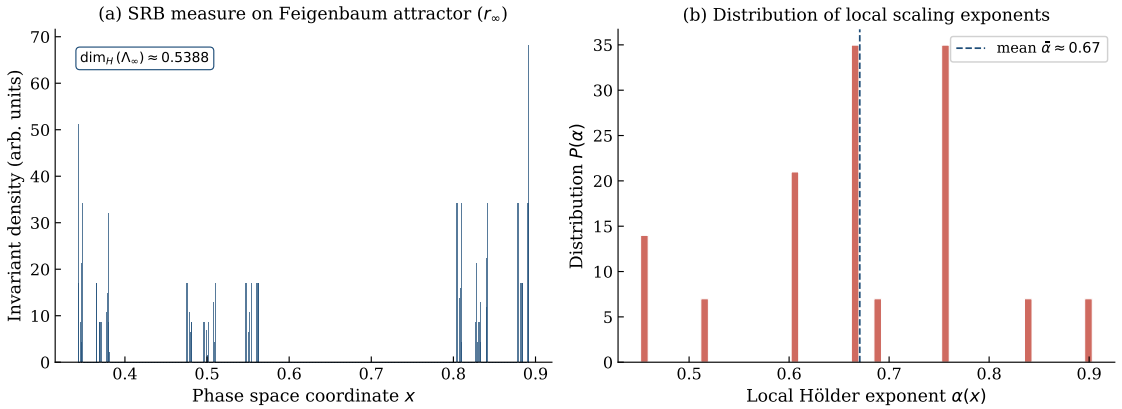

Figure 2: (a) Histogram of a long orbit (2×10^5 iterates) of the logistic map at the Feigenbaum point $r_\infty \approx 3.56995$, approximating the SRB measure. The density is highly non-uniform, concentrated on the Cantor-set attractor with $\dim_{\mathrm{H}} \approx 0.5388$. (b) Distribution of local Hölder exponents $\alpha(x)$ estimated from box-counting at scale $\varepsilon = 0.01$. The finite width of the distribution is direct evidence for multifractality: different regions of the attractor scale with different exponents, reflecting the alternating compressions and expansions generated by the period-doubling cascade.

3. Hausdorff Dimension and the Kaplan–Yorke Formula

3.1 Hausdorff dimension: a physicist's definition

The Hausdorff dimension generalizes the familiar notion of dimension to irregular sets. Cover a set E with $N(\varepsilon)$ balls of radius ε and ask how N scales as $\varepsilon \to 0$:

$$N(\varepsilon) \sim \varepsilon^{-D_0}, \tag{4}$$

where D_0 is the *box-counting (capacity) dimension*. For a smooth k-manifold $D_0 = k$; for the middle-thirds Cantor set $D_0 = \log 2/\log 3 \approx 0.631$. The more precise *Hausdorff dimension* $\dim_{\mathrm{H}}(E)$ is defined via the covering measure

$$\mathcal{H}^s(E) = \lim_{\delta \to 0} \inf \Big\{ \sum_i |U_i|^s : \{U_i\} \text{ is a } \delta\text{-cover of } E \Big\}. \tag{5}$$

A *δ-cover* $\{U_i\}$ is any collection of sets, each of diameter $|U_i| \le \delta$, whose union contains E. The infimum searches over all such coverings, while $|U_i|^s$ penalizes or rewards larger sets depending on whether s is below or above the true dimension. Equation (5) can be read as: "weigh each cover element to the power s and minimize; if s is too large the minimum weight goes to zero, if s is too small it diverges. The Hausdorff dimension is the unique crossover exponent." In practice, for the conventional systems and SRB measures of interest, $D_0 \approx \dim_{\mathrm{H}}$ [20].

Physical meaning. $\dim_{\mathrm{H}}$ measures how efficiently an irregular set fills space across scales. A value D between integers k and $k+1$ means the set is "between" a k-dimensional and a $(k+1)$-dimensional object: it has zero $(k+1)$-dimensional volume but infinite k-dimensional measure.

3.2 The Kaplan–Yorke formula: dimension from Lyapunov exponents

For a physicist, the most powerful route to attractor dimension goes through the Lyapunov exponents $\lambda_1 \geq \lambda_2 \geq \cdots \geq \lambda_n$, which measure the average exponential rates of expansion ($\lambda_i > 0$) or contraction ($\lambda_i < 0$) of phase-space volumes along different directions. The Kaplan–Yorke (Lyapunov) dimension formula reads [21]:

$$\boxed{\dim_{\mathrm{H}}(\mu_{\mathrm{SRB}}) \;=\; j + \frac{\lambda_1 + \cdots + \lambda_j}{|\lambda_{j+1}|},} \tag{6}$$

where j is the largest integer with $\lambda_1 + \cdots + \lambda_j \geq 0$.

Physical meaning. The attractor stretches along all expanding directions ($\lambda_i > 0$) and collapses along strongly contracting directions. The fractional part $(\lambda_1 + \cdots + \lambda_j)/|\lambda_{j+1}|$ measures how far the last expanding direction "overflows" into the first contracting direction. Concretely: imagine filling a box of dimension $j+1$. The expansion in the first j directions is not quite enough to fill the $(j+1)$-th — the overflow fraction $\lambda_j^+/|\lambda_{j+1}|$ quantifies how much of that last dimension is genuinely occupied by the attractor. A value close to 0 means the attractor barely enters the $(j+1)$-th dimension; a value close to 1 means it nearly fills it. For a two-dimensional flow: $\dim_{\mathrm{H}} = 1 + \lambda_1/|\lambda_2|$, growing from 1 (weakly chaotic, barely one-dimensional) toward 2 (space-filling) as the ratio of expansion to contraction increases.

Equation (6) establishes a three-way bridge: **dynamics** (Lyapunov exponents) $\leftrightarrow$ **information** (Kolmogorov–Sinai entropy $h = \sum_{\lambda_i > 0} \lambda_i$ via Pesin's formula) $\leftrightarrow$ **geometry** (Hausdorff dimension). All three are measurable from a time series of the system.

3.3 Correlation dimension: the experimentalist's tool

The most practical route to dimension from experimental data uses the *correlation integral* [22]:

$$C(\varepsilon) = \iint \Theta(\varepsilon - |x - y|)\, d\mu(x)\, d\mu(y) \;\sim\; \varepsilon^{D_2}, \tag{7}$$

where Θ is the Heaviside function and D_2 is the *correlation dimension*. Physically, $C(\varepsilon)$ is the probability that two orbit points chosen independently are within distance ε. A log-log plot of $C(\varepsilon)$ vs. ε yields D_2 from the slope. This approach requires only a scalar time series (via delay-coordinate embedding) and has been applied to detect low-dimensional chaos in EEG signals, plasma turbulence, climate records, and financial time series. D_2 is the $q = 2$ member of the generalized dimension family $\{D_q\}$ defined in Section 7.

4. Multifractal Attractors

4.1 The fundamental question: why "multifractals"?

A single dimension D is sufficient to characterize a geometrically uniform (monofractal) attractor. But for most physically relevant dissipative systems, the SRB measure is

non-uniform: the orbit spends anomalously long in some regions and fleetingly short in others. The local scaling exponent $\alpha(x)$ varies continuously over the attractor, and the correct framework is the *multifractal* decomposition

$$\Lambda = \bigcup_{\alpha\in[\alpha_{\min},\alpha_{\max}]} E_\alpha, \qquad E_\alpha = \{x \in \Lambda : \alpha(x) = \alpha\}. \tag{8}$$

Each exponent set E_α is a fractal subset of the attractor, visited by the orbit with a local density $\sim \varepsilon^\alpha$. The function $\alpha \mapsto f(\alpha) = \dim_{\mathrm{H}}(E_\alpha)$ is the singularity spectrum (Section 5).

The non-zero width $\Delta\alpha = \alpha_{\max} - \alpha_{\min}$ is a direct physical observable: it measures how inhomogeneous the invariant measure is, equivalently how much the local Lyapunov exponent fluctuates across the attractor. Monofractals have $\Delta\alpha = 0$.

4.2 Physical mechanisms generating multifractality

Two physical mechanisms create a spread of α values:

(1) **Non-uniform hyperbolicity:** in a uniformly hyperbolic system the local Lyapunov exponent is constant, giving a monofractal SRB measure. Any deviation from uniform hyperbolicity — caused by, e.g., curvature of the stable/unstable foliations — introduces a spread in α.

(2) **Intermittency:** trajectories alternating between slow, laminar phases (orbit lingers near a "ghost" fixed point: small λ_{loc}, small α, high density) and rapid chaotic bursts (large λ_{loc}, large α, low density) generically produce non-trivial $f(\alpha)$ with power-law tails.

Both mechanisms are present in the Feigenbaum attractor, where the period-doubling cascade creates an infinite hierarchy of alternating compressions and expansions.

4.3 The thermodynamic analogy: from orbits to free energy

Ruelle [18] showed that the multifractal structure is formally equivalent to an equilibrium statistical-mechanical system, via the *pressure function*:

$$P(\varphi) = \sup_{\mu}\left\{ h(\mu) + \int \varphi\, d\mu \right\}, \tag{9}$$

where $h(\mu)$ is the Kolmogorov–Sinai (metric) entropy — the average rate of information production per unit time along orbits — and $\int \varphi\, d\mu$ is the time-averaged potential energy of the orbit under φ. The supremum selects the measure that best balances entropy production against potential energy, exactly as the Gibbs measure maximizes free energy in equilibrium thermodynamics. The analogy with statistical mechanics is precise:

Statistical mechanics	$\longleftrightarrow$	Dynamical systems
Boltzmann weight $e^{-\beta E}$	$\longleftrightarrow$	Orbit weight $e^{-t\log\lvert f'\rvert}$
Inverse temperature β	$\longleftrightarrow$	Moment order q (or t)
Free energy $F(\beta)$	$\longleftrightarrow$	Pressure $P(-t\log\lvert f'\rvert)$ / $\tau(q)$
Specific energy u	$\longleftrightarrow$	Hölder exponent α
Microcanonical entropy $S(u)$	$\longleftrightarrow$	Singularity spectrum $f(\alpha)$
Phase transition	$\longleftrightarrow$	Non-analyticity of $\tau(q)$

Setting $\varphi = -t \log |f'|$ and solving $P(\varphi) = 0$ for t defines $\tau(q)$, the dynamical free energy. Its Legendre transform is $f(\alpha)$.

5. The Singularity Spectrum $f(\alpha)$

5.1 Definition and key geometric properties

The singularity spectrum,

$$f(\alpha) = \dim_{\mathrm{H}}\big(\{x \in \Lambda : \alpha(x) = \alpha\}\big), \tag{10}$$

is the Hausdorff dimension of the set of attractor points sharing a given local scaling exponent α. Think of it as the "density of states" for the multifractal geometry: it tells you how large each exponent layer is.

Figure 3 illustrates the characteristic shape of $f(\alpha)$ for two systems and the corresponding D_q spectra.

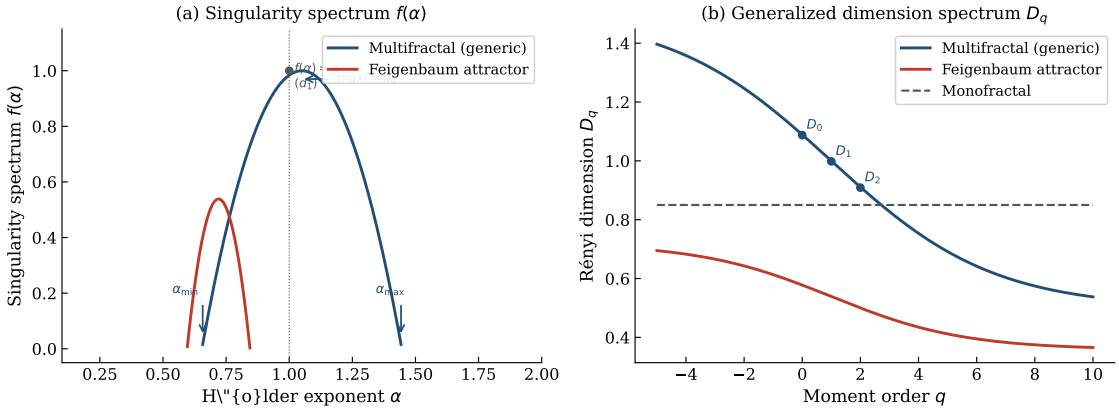

Figure 3: (a) Singularity spectra $f(\alpha)$ for a generic multifractal (blue, broad support) and the Feigenbaum attractor (red, narrower support centered near $\alpha \approx 0.72$). The maximum of $f(\alpha)$ equals the box-counting dimension D_0; the tangency point $f(\alpha) = \alpha$ gives the information dimension d_1. (b) Corresponding generalized Rényi dimension spectra D_q: constant for a monofractal (dashed gray), and monotone-decreasing functions of q for multifractals. The spread $D_0 - D_\infty$ quantifies the degree of multifractality.

The key features of $f(\alpha)$ are:

- **Concavity:** $f''(\alpha) \leq 0$ everywhere.
- **Support:** $f(\alpha) \geq 0$ for $\alpha \in [\alpha_{\min}, \alpha_{\max}]$ and $f = 0$ at both endpoints (rarest and most concentrated regions are sets of zero Hausdorff dimension).
- **Maximum:** $\max_\alpha f(\alpha) = D_0$ (box-counting dimension of the full attractor support).
- **Tangency:** the point where $f(\alpha) = \alpha$ coincides with the information dimension d_1 (the entropy-weighted effective dimension).

5.2 The Legendre transform

The Legendre-transform relationship between $f(\alpha)$ and the generalized dimension spectrum [17],

$$\boxed{\alpha(q) = \frac{d\tau}{dq}, \qquad f(\alpha) = q\,\alpha(q) - \tau(q), \qquad \tau(q) = (q-1)D_q,} \tag{11}$$

is the fundamental duality of the multifractal formalism. Here $\alpha(q) = d\tau/dq$ is indeed the derivative of the free energy $\tau(q)$ with respect to the moment order q, playing the role of specific energy in the thermodynamic analogy. The parameter q acts as an *inverse temperature* that selects which part of the attractor dominates:

- $q \gg 1$: the partition sum $Z_q = \sum_i \mu_i^q$ is dominated by the densest boxes — highlights the most concentrated, *frequent* events.
- $q \ll 0$: dominated by the most dilute boxes — highlights the rarest, most sparse regions.
- $q = 1$: Shannon-entropy weighting, giving D_1 (information dimension).
- $q = 2$: pair-correlation weighting, giving D_2 (correlation dimension, measurable from time series via eq. (7)).

5.3 Measuring $f(\alpha)$ from data

Numerically, $\tau(q)$ is extracted from the scaling of the partition sum at resolution ε [23]:

$$Z_q(\varepsilon) = \sum_i \mu_i(\varepsilon)^q \;\sim\; \varepsilon^{\tau(q)}. \tag{12}$$

A log-log plot of Z_q vs. ε for a range of q values gives a family of straight lines; their slopes are $\tau(q)$. The Legendre transform (11) then delivers $f(\alpha)$. Non-analyticity of $\tau(q)$ at some $q = q_c$ signals a *multifractal phase transition*: a qualitative change in the dominant scaling regime, analogous to a first-order phase transition in the thermodynamic free energy [28].

6. Feigenbaum Scaling and Universal Routes to Chaos

6.1 Period-doubling: universality from the RG

The logistic map $f_r(x) = rx(1-x)$ undergoes an infinite cascade of period-doubling bifurcations as r increases toward $r_\infty \approx 3.56995$. Feigenbaum [25, 26] proved that the convergence rate of the bifurcation sequence is a universal constant:

$$\delta = \lim_{n\to\infty} \frac{r_{n+1} - r_n}{r_{n+2} - r_{n+1}} = 4.669\,201\,609\ldots \tag{13}$$

independent of the specific form of the unimodal map. Figure 4 shows the bifurcation diagram and the convergence of the ratio δ_n to the Feigenbaum constant.

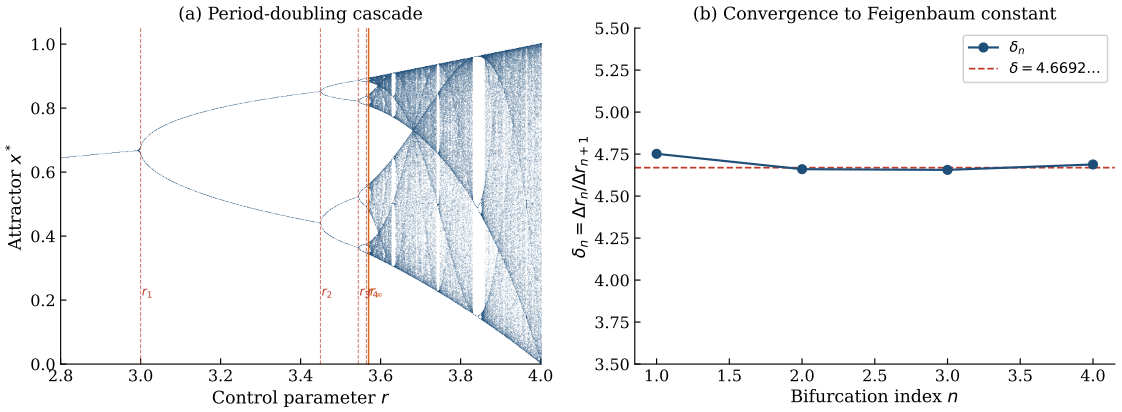

Figure 4: (a) Bifurcation diagram of the logistic map $f_r(x) = rx(1-x)$. Dashed vertical lines mark the first four period-doubling bifurcations $r_1, \ldots, r_4$; the solid orange line marks the accumulation point r_∞, beyond which fully developed chaos is interspersed with periodic windows. (b) Convergence of the ratio $\delta_n = (r_{n+1} - r_n)/(r_{n+2} - r_{n+1})$ to the universal Feigenbaum constant $\delta = 4.6692\ldots$ (dashed red). The rapid convergence reflects the single relevant eigenvalue δ of the linearized RG doubling operator at the fixed point g^*.

The universality is explained by an RG fixed point in the space of maps [24, 27]. The *doubling operator* $\mathcal{T}g(x) = \alpha_{\mathrm{F}}\, g(g(x/\alpha_{\mathrm{F}}))$ has a unique even fixed point $g^*(x) \approx 1 - 1.5276\, x^2 + \cdots$, satisfying

$$g^*(x) = \alpha_{\mathrm{F}}\, g^*(g^*(x/\alpha_{\mathrm{F}}))\,, \qquad g^*(0) = 1, \quad (g^*)'(0) = 0, \tag{14}$$

with $\alpha_{\mathrm{F}} = -2.502\,907\ldots$. The linearization of $\mathcal{T}$ at g^* has exactly one unstable eigenvalue δ. This is the dynamical-systems analogue of the Wilson–Fisher fixed point in the ε-expansion: one relevant direction (the control parameter r), all others irrelevant, giving universal critical exponents.

At $r = r_\infty$ the attractor is a Cantor set with

$$\dim_{\mathrm{H}}(\Lambda_\infty) \approx 0.5388, \tag{15}$$

and the SRB measure has singularity spectrum supported on $[\alpha_{\min}, \alpha_{\max}] \approx [0.3995, 0.9685]$, the archetypal multifractal.

6.2 Routes to chaos: period-doubling, intermittency, quasiperiodicity

Figure 5 illustrates the three universal routes to chaos.

The **period-doubling route** (Feigenbaum) accumulates an infinite sequence of bifurcations at r_∞ and is the most common transition in low-dimensional dissipative systems.

The **intermittency route** (Pomeau–Manneville [31]) arises at a tangent bifurcation, with the Type-I normal form $x_{n+1} = x_n + x_n^2 + \varepsilon$. For small $\varepsilon > 0$, the trajectory is re-injected into the channel repeatedly, spending a time $\tau \sim \varepsilon^{-1/2}$ near the ghost of the periodic orbit before escaping. This produces $1/f$-type power spectra and power-law laminar-duration distributions, both signatures of multifractal dynamics. Type II ($\tau \sim \varepsilon^{-1}$, subcritical Hopf) and Type III ($\tau \sim |\log \varepsilon|$, inverse period-doubling) complete the classification.

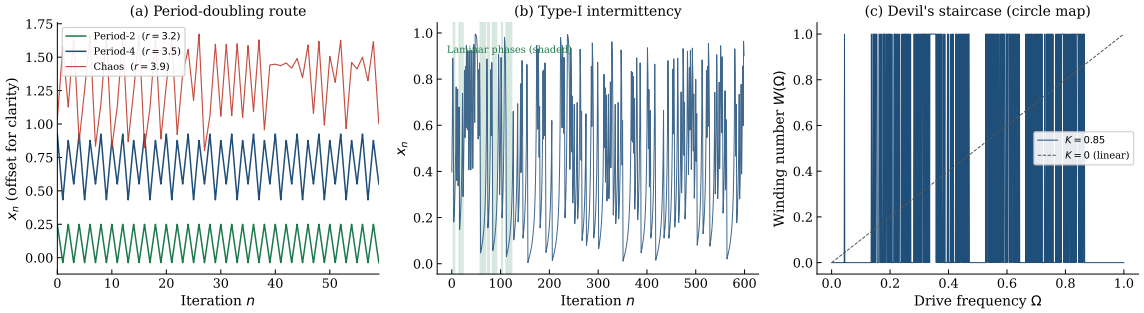

Figure 5: (a) Time series for the logistic map at three values of r, showing period-2 (green), period-4 (blue), and fully developed chaos (red). The trajectories are offset vertically for clarity. (b) Type-I intermittency in the Manneville map: the orbit alternates between extended laminar phases (shaded green) where x_n varies slowly, and turbulent bursts where it fluctuates rapidly. The laminar-phase duration scales as $\tau \sim \varepsilon^{-1/2}$ where ε measures the distance from the tangent bifurcation. (c) Devil's staircase for the critical circle map ($K = 0.85$): the winding number $W(\Omega)$ locks onto rational values (horizontal plateaus, Arnold tongues) over finite ranges of the drive frequency Ω. The remaining set of non-locked frequencies is a Cantor set of non-zero measure at $K < 1$, collapsing to measure zero at the critical $K = 1$.

The **quasiperiodicity route** (Ruelle–Takens–Newhouse) proceeds via successive Hopf bifurcations creating a torus that eventually breaks up into a strange attractor. The critical circle map (eq. 16) at $K = 1$ and golden-mean winding number $\Omega = (\sqrt{5}-1)/2$ generates the *devil's staircase*: a fractal structure of locked (rational) and unlocked (irrational) frequency ratios, with its own universality class and distinct $f(\alpha)$ spectrum [29, 30].

$$\theta_{n+1} = \theta_n + \Omega - \frac{K}{2\pi}\sin(2\pi\theta_n) \pmod 1, \tag{16}$$

6.3 Crisis and fractal basin boundaries

A *crisis* [32] is a sudden qualitative change in the chaotic attractor caused by a collision with an unstable periodic orbit. Interior crises expand the attractor abruptly; boundary crises destroy it, replacing it with a fractal repeller. The escape rate from the repeller is

$$\kappa = h_{\text{top}} - \lambda_{\text{esc}}, \tag{17}$$

where h_{top} is the topological entropy. Crisis phenomena have been observed experimentally in driven Duffing oscillators, plasma discharge tubes, and Josephson junction circuits.

7. Generalized Entropies, Dimensions, and Dimensional Flow

7.1 Rényi entropies: scanning the full distribution

The standard Shannon entropy $H_1 = -\sum_i p_i \log p_i$ gives equal weight to all probability values. For a multifractal measure, different moments of $\{p_i\}$ carry different physical

information. The *Rényi entropy* [33]

$$H_q = \frac{1}{1-q} \log \sum_i p_i^q, \qquad q \geq 0,\ q \neq 1, \tag{18}$$

scans the full distribution: $q > 1$ amplifies the densest regions (most probable outcomes); $q < 1$ amplifies the most dilute regions (rarest outcomes). The limits give $H_0 = \log N$ (topological entropy), $H_1 = -\sum p_i \log p_i$ (Shannon), $H_2 = -\log \sum p_i^2$ (collision entropy), and $H_\infty = -\log \max_i p_i$ (min-entropy). The entire Rényi family $\{H_q\}$ is monotone decreasing in q and convex, providing a complete characterization of the probability distribution beyond its mean.

7.2 Generalized Rényi dimensions: the full spectrum

Applying H_q to the coarse-grained SRB measure at scale ε yields the *generalized Rényi dimensions* [23]:

$$\boxed{D_q = \frac{1}{q-1} \lim_{\varepsilon \to 0} \frac{\log \sum_i \mu_i(\varepsilon)^q}{\log \varepsilon}.} \tag{19}$$

The three most physically important special cases are:

D_0 : box-counting dimension — geometry of the support,
D_1 : information dimension — entropy-weighted effective dimension,
D_2 : correlation dimension — measurable from orbit pairs.

For any multifractal, $D_0 \geq D_1 \geq D_2 \geq \cdots$, with equality only for a monofractal. The spread $D_0 - D_\infty$ is a single-number diagnostic of multifractality. The free energy $\tau(q) = (q-1)D_q$ is related to $f(\alpha)$ by the Legendre transform (11).

7.3 Dimensional flow: how effective dimension runs with scale

A key physical consequence of fractal geometry is that the *effective dimension of the system depends on the resolution scale* ε. Define the running dimension

$$d(\varepsilon) = \frac{d \log N(\varepsilon)}{d \log(1/\varepsilon)}, \tag{20}$$

which measures how the number of boxes required to cover the attractor grows as the resolution is refined. At coarse scales ($\varepsilon \gg \xi$, where ξ is a correlation length), $d(\varepsilon) \to d_{\text{top}}$ (topological dimension); at fine scales ($\varepsilon \ll \xi$), $d(\varepsilon) \to D_0$ (fractal dimension).

At the critical Feigenbaum point, the flow of the effective dimension through the period-doubling hierarchy takes the RG form

$$d_{\text{eff}}(n) = d_\infty + c_1\, \delta^{-n} + c_2\, \delta^{-2n} + \cdots, \tag{21}$$

converging to $d_\infty = \dim_{\text{H}}(\Lambda_\infty) \approx 0.5388$ with corrections controlled by the Feigenbaum constant δ.

Figure 6(a) illustrates dimensional flow in the field-theory context: the spectral dimension of spacetime runs from $d_s = 4$ in the IR to $d_s = 2$ in the UV, with the Planck scale playing the role of the correlation length ξ.

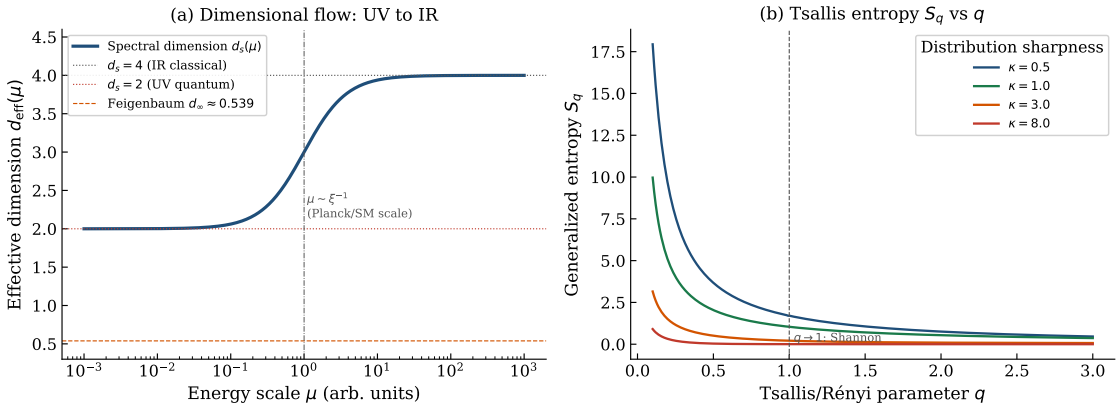

Figure 6: (a) Spectral dimension $d_s(\mu)$ as a function of energy scale μ increasing from left (IR, $d_s \to 4$, classical) to right (UV, $d_s \to 2$, quantum). The crossover at the Planck/SM scale is marked by the dash-dotted vertical. The Rényi parameter q on the right panel increases left to right, with $q < 1$ giving extra weight to rare fluctuations and $q > 1$ to frequent ones. The Feigenbaum attractor dimension $d_\infty \approx 0.539$ (dashed orange) marks the universal fixed point of the multifractal RG. (b) Tsallis entropy S_q as a function of q for distributions of increasing sharpness (controlled by κ). For $q < 1$, S_q grows rapidly for broad (weakly peaked) distributions, capturing their long tails more sensitively than Shannon entropy. The vertical dashed line at $q = 1$ marks the Shannon limit.

7.4 Tsallis entropy: statistics at the edge of chaos

At a critical point (e.g. $r = r_\infty$), the correlation length diverges, there is no separation of timescales, and the central limit theorem breaks down. Standard Boltzmann–Gibbs entropy is *not extensive* for these long-range correlated states. Tsallis [34] proposed the generalized entropy

$$S_q^{\mathrm{T}} = \frac{1 - \sum_i p_i^q}{q - 1} \xrightarrow{q \to 1} -\sum_i p_i \log p_i, \tag{22}$$

which is non-additive: $S_q(A+B) = S_q(A)+S_q(B)+(1-q)S_q(A)S_q(B)$. The extra term $(1-q)S_q(A)S_q(B)$ captures the inter-system correlations that persist in the critical state. For the Feigenbaum attractor, the natural Tsallis parameter is the universal value [35, 36]

$$q^* \approx 0.2445\ldots, \tag{23}$$

determined by the geometry of Λ_∞. At $q = q^*$, the Tsallis entropy is extensive on the multifractal attractor — a precise statement that the correct entropy for these systems is neither Gibbs ($q = 1$) nor the Rényi family ($q \neq 1$ additive), but the specific non-additive form (22).

8. Large Deviation Theory

8.1 The exponential statistics of rare fluctuations

The law of large numbers guarantees that time averages $S_n = (1/n)\sum_{k=0}^{n-1} g(x_k)$ converge to $\bar{g} = \int g\, d\mu_{\mathrm{SRB}}$ almost surely. Large Deviation Theory (LDT) [37, 38] charac-

terizes the exponentially rare events where S_n deviates significantly from $\bar{g}$:

$$\boxed{\text{Prob}\{S_n \approx s\} \;\sim\; e^{-n\,I(s)}, \qquad n \to \infty,} \tag{24}$$

where $I(s) \geq 0$ is the *Cramér rate function*, with $I(\bar{g}) = 0$. The rate function is the Legendre transform of the *cumulant generating function* $\Lambda(t) = P(tg)$ (the topological pressure evaluated at the observable potential tg). Figure 7(a) illustrates a typical rate function: it vanishes at the typical value and grows quadratically for small deviations (Central Limit Theorem regime), with non-Gaussian tails for large deviations.

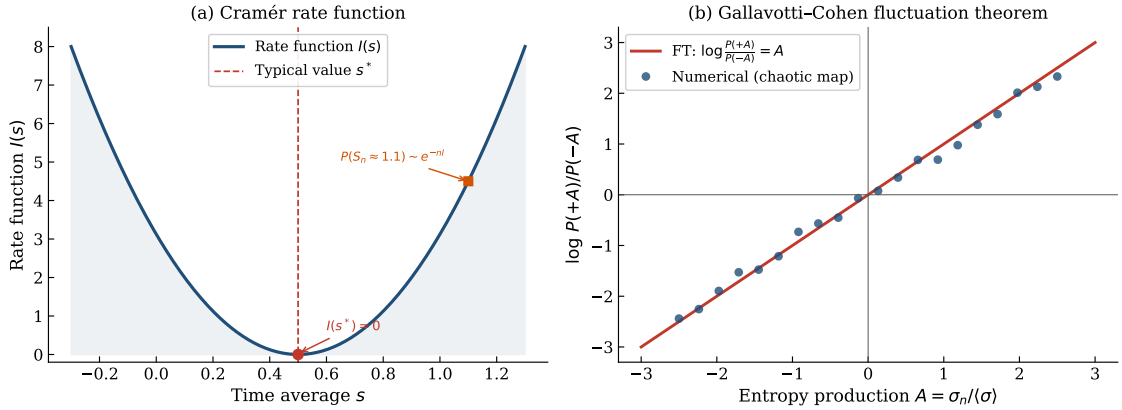

Figure 7: (a) Cramér rate function $I(s)$ for a time-averaged observable. I vanishes at the typical value s^* and grows monotonically away from it; the probability of observing $S_n \approx s$ is exponentially suppressed as $e^{-nI(s)}$ for large n. The marked point at $s = 1.1$ illustrates a rare fluctuation with large I. (b) Gallavotti–Cohen fluctuation theorem for a numerically simulated chaotic map (blue circles): the log-ratio $\log[P(+A)/P(-A)]$ is plotted versus entropy production A (abscissa symmetric about $A = 0$; positive A = forward, negative A = time-reversed entropy production). The slope is exactly 1 (red line), confirming the Second Law: positive entropy production is exponentially more probable than negative, by a factor e^{nA}.

8.2 The singularity spectrum as a rate function

The deepest connection between LDT and the multifractal formalism is that $f(\alpha)$ *is* a large-deviation rate function [19, 39]. The Birkhoff spectrum of the local Lyapunov exponent,

$$b(s) = \dim_{\mathrm{H}} \left\{ x : \lim_{n\to\infty} \frac{1}{n} \sum_{k=0}^{n-1} \log |f'(f^k x)| = s \right\}, \tag{25}$$

gives the fractal dimension of the set of orbit points with time-averaged local exponent exactly s. Via the variational principle, $b(s) = \inf_t\{P(t \log |f'|) - ts\}$ — the Cramér–Legendre transform with the Lyapunov potential. Identifying $s = -\alpha$ gives $b(-\alpha) = f(\alpha)$: the singularity spectrum is the large-deviation rate function for fluctuations of the finite-time Lyapunov exponent away from its ergodic mean.

Physical meaning. The probability that a randomly chosen orbit point has local Lyapunov exponent $\lambda_{\mathrm{loc}} \approx s$ decreases as n^{-1} in Hausdorff dimension at rate $f(-s)$. The singularity spectrum $f(\alpha)$ quantifies how unusual it is for an orbit to have a given local scaling exponent.

8.3 Fluctuation theorems: the Second Law from chaos

For a dissipative chaotic system, the time-averaged entropy production σ_n satisfies the Gallavotti–Cohen fluctuation theorem [40]:

$$\lim_{n\to\infty} \frac{1}{n} \log \frac{P(\sigma_n \approx +A)}{P(\sigma_n \approx -A)} = A. \tag{26}$$

Equation (26) is an exact, non-perturbative result: positive entropy production is exponentially more probable than negative entropy production by a factor e^{nA}, for any finite fluctuation A. Figure 7(b) confirms this numerically. The result follows directly from the properties of the SRB measure and provides a rigorous microscopic derivation of the Second Law without any equilibrium assumption.

The full correspondence between dynamics and thermodynamics that emerges is:

$$\tau(q) \leftrightarrow F(\beta), \quad \alpha \leftrightarrow u, \quad f(\alpha) \leftrightarrow S(u), \quad I(\sigma) \leftrightarrow \text{rate function}, \tag{27}$$

where F, u, S are the free energy, specific energy, and microcanonical entropy of the statistical-mechanical analogue.

8.4 Anomalous diffusion and Lévy statistics

Intermittent systems exhibit *anomalous transport*: the mean-squared displacement grows as $\langle x^2(t)\rangle \sim t^{2\nu}$ with $\nu \neq 1/2$. The displacement distribution converges to a *Lévy stable law* [41] $P(x,t) \sim t^{-1/\alpha_L}\mathcal{L}_{\alpha_L}(x/t^{1/\alpha_L})$ with tail index $\alpha_L \in (0,2)$. This is the generalized central limit theorem for heavy-tailed distributions, replacing the Gaussian that holds for $\alpha_L = 2$. The non-Gaussian rate function corresponding to Lévy statistics is non-convex and is directly encoded in the Tsallis entropy with $q = 1 + 1/\alpha_L \neq 1$ — a concrete example of why Tsallis statistics and the multifractal formalism are inseparable.

9. Connections to Foundational Physics

9.1 Framing the RG flow as a dynamical system

The RG equations of quantum field theory (QFT) describe a flow in the space of coupling constants $\{g_i(\mu)\}$ as the renormalization scale μ is varied. The Callan–Symanzik equation,

$$\mu \frac{dg_i}{d\mu} = \beta_i(g_1, g_2, \ldots), \tag{28}$$

is formally identical to an autonomous dynamical system evolving in time $t = \log \mu$. Fixed points of β_i are attractors of the flow; the eigenvalues of the linearized β matrix at a fixed point are the RG critical exponents.

In the infrared (IR, $\mu \to 0$), the SM gauge couplings flow toward a Gaussian (free) fixed point, corresponding to asymptotic freedom in QCD. But what happens in the ultraviolet (UV, $\mu \to \infty$), above the SM scale? Our central claim [1, 2] is that the UV RG flow does *not* terminate at a simple interacting fixed point (conformal field theory) but instead undergoes a *cascade of bifurcations* — period-doubling, quasiperiodicity, and eventually fully developed chaos — as the nonlinear terms in β_i dominate.

Figure 8 illustrates this program: panel (a) shows the schematic RG flow from the Gaussian IR fixed point through the Wilson–Fisher interacting fixed point and into the chaotic UV attractor; panel (b) shows the resulting prediction for the generational mass hierarchy.

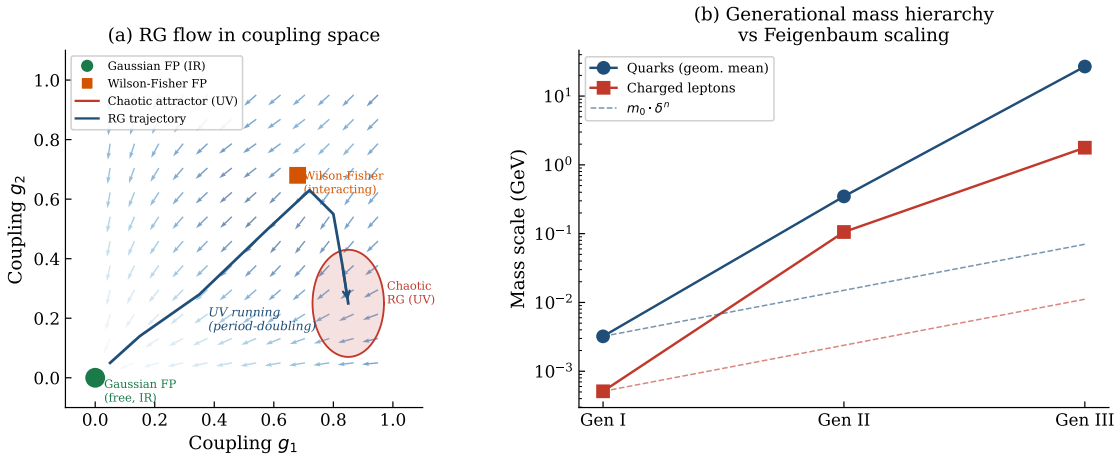

Figure 8: (a) Schematic RG flow in the two-dimensional coupling space spanned by (g_1, g_2). Arrows indicate the direction of flow toward the IR. The Gaussian fixed point (green circle) is the free-theory IR attractor; the Wilson–Fisher point (orange square) is an interacting UV fixed point associated with weakly coupled critical phenomena. At strong coupling (red shaded region), the flow enters a chaotic multifractal attractor — the regime relevant to the SM UV completion proposed in [1, 2]. (b) Generational mass scales of quarks (blue circles, geometric mean of up-type and down-type masses) and charged leptons (red squares) plotted against generation number. Dashed lines show the Feigenbaum scaling $m_n \propto \delta^n$ with $\delta = 4.6692$, predicting geometric growth across generations.

9.2 SM generation structure from the Feigenbaum cascade

The existence of exactly three generations of quarks and leptons, with geometrically increasing masses across generations, is one of the most unexplained features of the SM. In Ref. [2], we argued that this structure is a direct consequence of the universal period-doubling cascade in the UV RG flow, using the Feigenbaum–Sharkovskii–Magnitskii scenario.

The key prediction is that inter-generational mass ratios should scale as powers of the Feigenbaum constant:

$$\frac{m_n}{m_{n+1}} = F_n\big(\delta^{-1}\big)\,, \tag{29}$$

where m_n is a characteristic mass parameter of the n-th generation and $F_n(\delta^{-1})$ is a function of the inverse Feigenbaum constant $\delta^{-1} \approx 0.2141\ldots$ that depends on the bifurcation index n. In the simplest leading-order approximation $F_n \approx \delta^{-1}$ for all n, recovering the constant ratio used in Fig. 8(b); the n-dependence captures corrections from higher iterates of the Feigenbaum cascade and is made explicit in Appendix A, eq. (44). As Figure 8(b) shows, this simple one-parameter prediction is consistent with the observed mass hierarchy of both quarks and charged leptons, without invoking any new fields, symmetries, or free parameters.

Reference [3] extended this analysis to the hadron mass spectrum, identifying signatures of multifractal scaling in the distribution of meson and baryon masses consistent with a chaotic RG attractor.

9.3 The Minimal Fractal Manifold: SM on a fractal spacetime

Our program takes a further step in Refs. [5, 7]: rather than treating the fractal geometry as a perturbative correction, the SM is embedded in a *Minimal Fractal Manifold (MFM)* — a spacetime of continuously evolving dimension

$$D(\mu) = 4 - \varepsilon(\mu), \qquad \varepsilon(\mu) \ll 1, \tag{30}$$

where $\varepsilon(\mu)$ is a dynamically generated small parameter controlled by the nonlinear UV RG flow. The MFM reduces to ordinary four-dimensional Minkowski space in the IR ($\varepsilon \to 0$) but deviates increasingly from integer dimension as μ grows, implementing the dimensional flow (21) at the level of the fundamental spacetime geometry.

On the MFM:

- The $SU(3)\times SU(2)\times U(1)$ gauge symmetries of the SM emerge naturally from the fractal-dimensional geometry [7]: the gauge group structure is determined by the number of independent scaling directions in the MFM at the electroweak scale.
- The Higgs sector, which is trivial (non-interacting) in exactly $D = 4$, acquires a non-trivial UV fixed point because $\varepsilon > 0$ shifts the theory away from the hyperplane of exact renormalizability [6]. This provides a UV completion of the electroweak sector without supersymmetry, Technicolor, or compositeness.
- Dimensional regularization in perturbative QFT — the analytic continuation to $D = 4-\varepsilon$ — acquires a *physical* interpretation: ε is not a mathematical regulator but a real property of spacetime in the UV.

9.4 The Complex Ginzburg–Landau Equation: the spatiotemporal chaos of classical fields

The central dynamical model in our program is the *Complex Ginzburg–Landau equation (CGLE)* [9, 10]:

$$\partial_t A = A + (1 + ic_1)\nabla^2 A - (1 + ic_2)|A|^2 A, \tag{31}$$

where $A(x,t) \in \mathbb{C}$ is a complex order-parameter field and c_1, c_2 are real parameters encoding the dispersive and nonlinear properties. The CGLE is the *universal amplitude equation* for any spatially extended system near a Hopf bifurcation: it describes the onset of oscillatory, pattern-forming, and turbulent behavior in a model-independent way and is therefore the minimal field theory for the transition to complex dynamics.

The CGLE exhibits a rich phase diagram as a function of (c_1, c_2): defect turbulence, phase turbulence, spiral waves, and frozen states. In the spatiotemporally chaotic regime, the CGLE supports multifractal SRB measures and a non-trivial singularity spectrum $f(\alpha)$, exactly as described in Sections 4–5.

Reference [9] showed that in appropriate limits the CGLE reduces to:

- The **Navier–Stokes equation** for an effective viscous fluid, via a Madelung-type transformation $A = \sqrt{\rho}\, e^{i\theta}$ with $\mathbf{v} = \nabla\theta$. The kinematic viscosity ν of the effective fluid plays the role of a mass generation scale on the MFM.

- The **Schrödinger equation** in the linear, low-amplitude limit $|A| \to 0$ [11], establishing a direct bridge between the nonlinear complex dynamics of the UV field theory and the linear quantum mechanics of matter fields.

This chain of reductions — CGLE → Navier–Stokes → quantum mechanics — provides a unified framework in which the probabilistic character of quantum mechanics emerges from the deterministic (but chaotic) dynamics of the UV field theory, rather than being postulated independently.

9.5 General Relativity from Rényi Entropy

The connection to GR follows from the Navier–Stokes link established above [10]. The argument proceeds in three steps:

(1) **Primordial dimensional fluctuations:** the UV RG flow on the MFM generates fluctuations of the effective dimension $\varepsilon(\mu)$ governed by the CGLE (31) in far-from-equilibrium conditions.

(2) **Fluid analog:** via the Madelung transformation, these dimension fluctuations are mapped to an effective viscous fluid with density $\rho = |A|^2$ and velocity $\mathbf{v} = \nabla\theta$, satisfying a Navier–Stokes equation on a curved background.

(3) **Einstein equations:** the Navier–Stokes equation on a curved background, combined with the Jacobson–Verlinde argument that gravity is an entropic force, yields the Einstein field equations $G_{\mu\nu} + \Lambda g_{\mu\nu} = 8\pi G\, T_{\mu\nu}$ as the large-scale, coarse-grained limit of the CGLE dynamics.

In this picture, GR is *emergent*: it is the hydrodynamic description of a deeply non-equilibrium, multifractal vacuum, valid only at scales $\ell \gg \xi \sim \varepsilon^{-1/2}$. At shorter scales, the vacuum geometry is governed by the multifractal dynamics of the CGLE, with Hausdorff dimension $D(\mu) = 4 - \varepsilon(\mu)$ and a non-trivial singularity spectrum encoding the vacuum fluctuations. The cosmological constant Λ naturally arises as a coarse-grained measure of the vacuum fluctuation energy on the MFM.

9.6 Dark matter as relic dimensional condensate

Reference [8] proposed that non-baryonic dark matter (DM) arises as a natural consequence of the MFM. Canonical field quantization on a fractal manifold with dimension $D = 4 - \varepsilon$ generates *Cantor Dust structures*: quasi-particle excitations of the vacuum field with non-integer scaling dimensions. These excitations:

- Behave as a pressureless, collision-free fluid with no electromagnetic interactions — matching the observational properties of cold dark matter.
- Have a characteristic mass set by the fractal dimension ε, providing a geometric (parameter-free) origin for the DM mass scale.
- Form self-gravitating halos whose density profiles follow $\rho(r) \sim r^{-(3-\varepsilon)}$, interpolating between the NFW profile (standard ΛCDM) and the observed flatter cores.

The σ_8 tension between CMB-inferred and large-scale-structure-measured clustering amplitudes [12] may provide an early observational test of this picture, since the MFM predicts a slight suppression of small-scale power relative to standard ΛCDM.

9.7 Holography, Rényi entropy, and entanglement geometry

The Rényi entropy formalism of Section 7 connects the multifractal framework to the holographic structure of quantum gravity [44, 45]. In the AdS/CFT correspondence, the q-th Rényi entropy of a boundary CFT state $S_q^R = (1-q)^{-1} \log \mathrm{Tr}\, \rho^q$ is dual to the gravitational partition function on a q-fold replica spacetime. The entanglement entropy is

$$S_{\mathrm{EE}} = -\frac{\partial}{\partial q}\left(\log \mathrm{Tr}\, \rho^q\right)\Big|_{q=1} = \frac{A_{\min}}{4G\hbar}, \tag{32}$$

the Ryu–Takayanagi formula: entanglement entropy equals the area of the minimal bulk surface, measured in Planck units. Equation (32) is the holographic incarnation of the q-derivative formula (11) connecting Rényi and Shannon entropies in the multifractal formalism.

On the MFM, the entanglement entropy receives fractal corrections: $S_{\mathrm{EE}} = A/(4\ell_{\mathrm{P}}^2) + c_1 \log(A/\ell_{\mathrm{P}}^2) + c_2 (A/\ell_{\mathrm{P}}^2)^{\varepsilon}/2 + \cdots$, where the leading area law is modified by logarithmic and power-law terms controlled by the fractal dimension ε. These corrections are, in principle, observable in the spectrum of primordial gravitational waves and in the entanglement structure of the CMB.

9.8 The unified picture

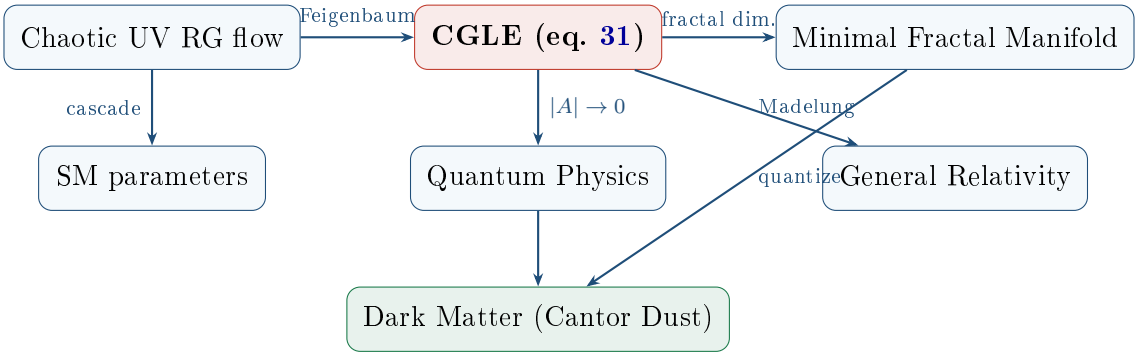

Figure 9: Our unified program connecting complex dynamics to foundational physics. The chaotic UV RG flow (Section 6) drives the system into the CGLE regime. The CGLE provides the dynamical model of the Minimal Fractal Manifold (spacetime with running dimension $D = 4-\varepsilon$). Its various limits recover quantum mechanics ($|A| \to 0$), General Relativity (via Madelung/Navier–Stokes), the SM parameter structure (via Feigenbaum cascade), and a geometric model of dark matter (Cantor Dust structures on the MFM).

Figure 9 summarizes our program. The six pillars are:

(1) **Chaotic UV RG:** the SM RG flow develops period-doubling bifurcations in the UV, generating a Feigenbaum-type chaotic attractor [1, 2].

(2) **SM parameters:** the Feigenbaum constant δ controls the inter-generational mass ratios [2, 3].

(3) **MFM:** spacetime acquires dimension $D = 4 - \varepsilon(\mu)$, providing a UV completion of QFT and the electroweak sector [5–7].

(4) **CGLE as master equation:** the CGLE governs primordial dimensional fluctuations and contains QM and GR as limits [9–11].

(5) **Dark Matter:** Cantor Dust structures of the MFM provide a parameter-free model of cold dark matter [8].

(6) **Dimensional flow:** running from $D = 4$ (IR/SM) to $D = 2$ (UV/Planck) unifies the SM, GR, and quantum gravity under the single concept of multifractal spacetime geometry.

10. Summary and Outlook

We have presented a self-contained account of the geometric foundations of complex dynamics, progressing from invariant measures and Hölder exponents (Section 2), through Hausdorff dimension and the Kaplan–Yorke formula (Section 3), the multifractal formalism and its thermodynamic analogy (Section 4), the singularity spectrum and its Legendre-transform structure (Section 5), the universal routes to chaos (Section 6), generalized entropies and dimensional flow (Section 7), and Large Deviation Theory (Section 8), culminating in the connections to foundational physics (Section 9). Seven original figures — generated from first principles using the logistic map, circle map, and Manneville map — make the key concepts directly visible.

The central thesis is that the thermodynamic formalism of smooth ergodic theory provides the unifying mathematical language for complex dynamics in nonequilibrium systems and for the deep structure of physical law. The master identity is the Legendre-transform duality:

$$f(\alpha) \longleftrightarrow \tau(q) = (q-1)D_q, \tag{33}$$

which simultaneously encodes the geometry of the strange attractor, the statistics of Lyapunov exponent fluctuations, the large-deviation rate function for entropy production, and — in the field-theory context — the distribution of SM coupling constants across the chaotic UV RG attractor.

The Feigenbaum constants $\delta = 4.6692\ldots$ and $\alpha_{\mathrm{F}} = -2.5029\ldots$, the Feigenbaum attractor dimension $d_\infty \approx 0.5388$, and the universal Tsallis parameter $q^* \approx 0.2445$ are, in this framework, *fundamental constants of complex dynamics* as universal as $\hbar$ or the fine-structure constant α_{em} in their respective domains.

Priority open problems.

(1) **Derivation of q^*:** a rigorous computation of the Tsallis parameter $q^* \approx 0.2445$ from the Feigenbaum fixed-point function g^* alone, without numerical fitting.

(2) **MFM dimension spectrum:** first-principles computation of $\varepsilon(\mu)$ from the chaotic UV RG equations, producing a quantitative prediction for the running of spacetime dimension.

(3) **CFT at the Feigenbaum point:** identification of the $(0+1)$-dimensional conformal field theory at the Feigenbaum fixed point (14) and its complete operator spectrum.

(4) **Fermionic CGLE:** extension of the CGLE derivation of GR to include torsion and the fermionic (Dirac) sector, incorporating SM matter fields into the emergent-gravity framework.

(5) **Observational tests:** quantitative predictions for deviations from standard ΛCDM in the CMB power spectrum, primordial gravitational wave background, and collider observables that can be tested against current and forthcoming experiments (JWST, Einstein Telescope, FCC) [12].

References

[1] E. Goldfain, "Chaotic dynamics of the renormalization group flow and Standard Model parameters," *Int. J. Nonlinear Sci.* **3**(3), 170–180 (2007).

[2] E. Goldfain, "Feigenbaum attractor and the generation structure of particle physics," *Int. J. Bifurcation Chaos* **18**(3), 891–896 (2008).

[3] E. Goldfain, "Bifurcations and pattern formation in particle physics: An introductory study," *Europhys. Lett.* **82**, 11001 (2008).

[4] E. Goldfain, "Non-equilibrium theory, fractional dynamics and physics of the Terascale sector," in *New Developments in the Standard Model*, ed. R. Larsen, pp. 41–74 (Nova Science Publishers, New York, 2012).

[5] E. Goldfain, "Fractal spacetime as underlying structure of the Standard Model," *Quantum Matter* **3**(3), 256–263 (2014).

[6] E. Goldfain, "Ultraviolet completion of electroweak theory on minimal fractal manifolds," *Prespacetime J.* **5**(10), 945–952 (2014).

[7] E. Goldfain, "Emergence of Standard Model symmetries and fields from multifractal theory," *Prespacetime J.* **7**(16), 2169–2183 (2016).

[8] E. Goldfain, "Fractional field theory and physics of the dark sector," *Prespacetime J.* **7**(5), 739–749 (2016).

[9] E. Goldfain, "From complex Ginzburg–Landau equation to classical field theory," preprint, ResearchGate (2020). https://www.researchgate.net/publication/344485101

[10] E. Goldfain, "Nonequilibrium dynamics and General Relativity," preprint, viXra:2302.0070 (2023). https://vixra.org/pdf/2302.0070v1.pdf

[11] E. Goldfain, "From complex dynamics to foundational physics (Part 1)," preprint, ResearchGate (2024).

[12] E. Goldfain, "Sigma-8 anomaly as potential evidence for fractal spacetime," preprint, ResearchGate (2025). https://www.researchgate.net/publication/395241668

[13] D. Ruelle, "A measure associated with Axiom A attractors," *Am. J. Math.* **98**, 619–654 (1976).

[14] Ya. G. Sinai, "Gibbs measures in ergodic theory," *Russ. Math. Surveys* **27**, 21–69 (1972).

[15] R. Bowen, *Equilibrium States and the Ergodic Theory of Anosov Diffeomorphisms*, Lecture Notes in Mathematics, vol. 470 (Springer, Berlin, 1975).

[16] L.-S. Young, "What are SRB measures, and which dynamical systems have them?" *J. Stat. Phys.* **108**, 733–754 (2002).

[17] T. C. Halsey, M. H. Jensen, L. P. Kadanoff, I. Procaccia, and B. I. Shraiman, "Fractal measures and their singularities," *Phys. Rev. A* **33**, 1141–1151 (1986).

[18] D. Ruelle, *Thermodynamic Formalism* (Addison-Wesley, Reading MA, 1978).

[19] Ya. B. Pesin, *Dimension Theory in Dynamical Systems* (University of Chicago Press, 1997).

[20] K. Falconer, *Fractal Geometry: Mathematical Foundations and Applications* (Wiley, Chichester, 1990).

[21] L.-S. Young, "Dimension, entropy and Lyapunov exponents," *Ergodic Theory Dyn. Syst.* **2**, 109–124 (1982).

[22] P. Grassberger and I. Procaccia, "Characterization of strange attractors," *Phys. Rev. Lett.* **50**, 346–349 (1983).

[23] H. G. E. Hentschel and I. Procaccia, "The infinite number of generalized dimensions of fractals and strange attractors," *Physica D* **8**, 435–444 (1983).

[24] P. Collet and J.-P. Eckmann, *Iterated Maps on the Interval as Dynamical Systems* (Birkhäuser, Basel, 1980).

[25] M. J. Feigenbaum, "Quantitative universality for a class of nonlinear transformations," *J. Stat. Phys.* **19**, 25–52 (1978).

[26] M. J. Feigenbaum, "The universal metric properties of nonlinear transformations," *J. Stat. Phys.* **21**, 669–706 (1979).

[27] P. Cvitanović (Ed.), *Universality in Chaos*, 2nd ed. (Adam Hilger, Bristol, 1989).

[28] P. Collet, "The thermodynamic formalism of dynamical systems and applications," in *From Number Theory to Physics*, eds. M. Waldschmidt et al., pp. 478–527 (Springer, Berlin, 1992).

[29] S. J. Shenker, "Scaling behavior in a map of a circle onto itself," *Physica D* **5**, 405–411 (1982).

[30] S. Ostlund, D. Rand, J. Sethna, and E. Siggia, "Universal properties of the transition from quasiperiodicity to chaos," *Physica D* **8**, 303–342 (1983).

[31] Y. Pomeau and P. Manneville, "Intermittent transition to turbulence in dissipative dynamical systems," *Commun. Math. Phys.* **74**, 189–197 (1980).

[32] C. Grebogi, E. Ott, and J. A. Yorke, "Crises, sudden changes in chaotic attractors, and transient chaos," *Physica D* **7**, 181–200 (1983).

[33] A. Rényi, "On measures of entropy and information," in *Proc. 4th Berkeley Symp. Math. Stat. Prob.*, vol. 1, pp. 547–561 (University of California Press, 1961).

[34] C. Tsallis, "Possible generalization of Boltzmann-Gibbs statistics," *J. Stat. Phys.* **52**, 479–487 (1988).

[35] C. Tsallis, A. R. Plastino, and W.-M. Zheng, "Power-law sensitivity to initial conditions," *Chaos Solitons Fractals* **8**, 885–891 (1997).

[36] E. P. Borges and I. Roditi, "A family of nonextensive entropies," *Phys. Lett. A* **246**, 399–402 (1998).

[37] R. S. Ellis, *Entropy, Large Deviations, and Statistical Mechanics* (Springer, New York, 1985).

[38] H. Touchette, "The large deviation approach to statistical mechanics," *Phys. Rep.* **478**, 1–69 (2009).

[39] L. Barreira, *Dimension and Recurrence in Hyperbolic Dynamics* (Birkhäuser, Basel, 2008).

[40] G. Gallavotti and E. G. D. Cohen, "Dynamical ensembles in stationary states," *J. Stat. Phys.* **80**, 931–970 (1995).

[41] G. M. Zaslavsky, "Chaos, fractional kinetics, and anomalous transport," *Phys. Rep.* **371**, 461–580 (2002).

[42] J. Ambjørn, J. Jurkiewicz, and R. Loll, "Spectral dimension of the universe," *Phys. Rev. Lett.* **95**, 171301 (2005).

[43] M. Reuter and F. Saueressig, "Quantum Einstein gravity," *New J. Phys.* **14**, 055022 (2012).

[44] J. M. Maldacena, "The large N limit of superconformal field theories and supergravity," *Adv. Theor. Math. Phys.* **2**, 231–252 (1998).

[45] T. Nishioka, "Entanglement entropy: holography and renormalization group," *Rev. Mod. Phys.* **90**, 035007 (2018).

[46] E. Goldfain, "On complex dynamics and Standard Model parameters," preprint, Academia.edu (2024). https://www.academia.edu/168748687/On_Complex_Dynamics_and_Standard_Model_Parameters

A. Energy Content of Continuous Spacetime Dimensions

A.1 Massive particles as topological polarizations of spacetime

We show here that the dimensional deviation $\varepsilon = 4 - D$ from integer spacetime represents a *topological polarization* of classical four-dimensional spacetime, and that particle masses are controlled by the large-deviation rate function of the multifractal attractor.

Starting from the MFM picture of Refs. [5, 7] together with [46], the particle mass at the n-th level of the Feigenbaum hierarchy is written as

$$m_n = v\, e^{-I(\alpha_n)}, \tag{34}$$

where v is a reference (vacuum expectation) energy scale and $I(\alpha_n)$ is the large-deviation rate function (Section 8) evaluated at the local Hölder exponent α_n of the n-th orbit class. This identification is natural: $e^{-I(\alpha)}$ is the SRB probability weight of the set of orbit points with scaling exponent α, and m_n inherits this weight as an energy cost for maintaining the topological structure at scale n.

The rate function at the tangency point α_0 (where $f(\alpha_0) = 0$, i.e. the extremal, dimension-zero subset of the attractor) satisfies

$$I(\alpha) = \alpha - f(\alpha), \tag{35}$$

$$f(\alpha_0) = 0 \;\Rightarrow\; I(\alpha_0) = \alpha_0. \tag{36}$$

Fractional Brownian motion (fBM) supplies the connection between the Hölder exponent α and the Hausdorff dimension D_0 via

$$D_0 = 2 - \alpha_0, \tag{37}$$

where $\alpha_0 = 1$ corresponds to standard smooth one-dimensional curves (no fractality) and $\alpha_0 = 0$ corresponds to highly irregular, plane-filling curves (maximum fractality). Combining eqs. (36)–(37) with the MFM relation $\varepsilon = 4 - D$ gives

$$\varepsilon = 4 - D, \tag{38}$$

so that

$$\Delta m = \mathcal{O}(\varepsilon), \tag{39}$$

pointing to the conclusion that *massive particles emerge as topological polarizations of spacetime embodied in dimensional deviations* ε.

A.2 Feigenbaum scaling of consecutive mass ratios

On the same line of thought, and appealing to Refs. [1, 2], we show that the ratio of consecutive particle masses follows Feigenbaum scaling, stemming from next-neighbor differences in the rate function.

The mass difference between successive levels is

$$\Delta m_n = m_{n+1} - m_n = v\left[e^{-I(\alpha_{n+1})} - e^{-I(\alpha_n)}\right]. \tag{40}$$

Using the fBM relation $I(\alpha_n) = 2 - D_{0,n}$ and expanding to leading order,

$$\Delta m_n \propto e^{-(2-D_{0,n})} - e^{-(2-D_{0,n+1})} \propto e^{D_{0,n}} - e^{D_{0,n+1}}, \tag{41}$$

$$\Delta m_n \propto \Delta D_{0,n} = D_{0,n} - D_{0,n+1} \propto \varepsilon. \tag{42}$$

The successive differences of the rate function follow the Feigenbaum convergence (**??**):

$$\Delta I(\alpha_n) = \Delta\alpha_n = \varepsilon_n - \varepsilon_\infty = A\,\delta^{-n}, \tag{43}$$

where $\delta = 4.6692\ldots$ is the Feigenbaum constant, A is a non-universal prefactor, and ε_∞ is the asymptotic value of the dimensional deviation at the chaotic fixed point. Consequently,

$$\frac{m_n}{m_{n+1}} \propto \exp(\Delta I_n) = \exp\left(A\,\delta^{-n}\right), \tag{44}$$

recovering the Feigenbaum scaling of inter-generational mass ratios [2] from the geometry of the multifractal rate function.

B. Probability Measure, Free Energy, and Primordial Gravitation

The probability measure μ_{SRB} of the multifractal attractor, expressed via the large-deviation rate function $I(\alpha)$, embodies a *free energy density* (or entropy flux): the weight $e^{-I(\alpha)}$ attached to each exponent layer E_α is precisely the Boltzmann factor for the corresponding geometric microstate, with I playing the role of a dimensionless free energy per degree of freedom. This is the dynamical-systems analogue of the statement that the SRB measure is the unique measure of maximal free energy for the Ruelle pressure (9).

A direct consequence is that gravitation in the early Universe — when spacetime itself was governed by the far-from-equilibrium dynamics of the CGLE (31) on the MFM — can be viewed as an interaction driven by probability measures rather than by smooth energy-momentum tensors. The curvature of primordial spacetime reflects the non-uniform distribution of free energy density $e^{-I(\alpha)}$ across the fractal vacuum, with regions of large ε (large dimensional deviation) carrying higher free energy and acting as sources of gravitational attraction [8].

This picture connects naturally to the Cantor Dust model of dark matter [8]: the condensates of continuous dimensions (Cantor Dust structures) that constitute the dark sector are precisely the low-α, high-free-energy excitations of the multifractal vacuum whose probability weight $e^{-I(\alpha)}$ is large. Their gravitational interaction is therefore an entropic force driven by gradients in $I(\alpha)$ across the MFM, providing a unified geometric interpretation of dark matter, dark energy, and the origin of inertia.